



UNIVERSITY OF LEEDS

This is a repository copy of *A Pneumatic Anchoring Mechanism for Improved Stability in Soft Magnetic Manipulators for Surgery*.

White Rose Research Online URL for this paper:

<https://eprints.whiterose.ac.uk/id/eprint/227518/>

Version: Accepted Version

Proceedings Paper:

Koszowska, Z., Brockdorff, M., Lloyd, P. et al. (2 more authors) (2025) A Pneumatic Anchoring Mechanism for Improved Stability in Soft Magnetic Manipulators for Surgery. In: 2025 IEEE 8th International Conference on Soft Robotics (RoboSoft). 2025 IEEE 8th International Conference on Soft Robotics (RoboSoft), 22-26 Apr 2025, Lausanne, Switzerland. IEEE ISBN 979-8-3315-2021-2

<https://doi.org/10.1109/robosoft63089.2025.11020815>

© 2025 IEEE. Personal use of this material is permitted. Permission from IEEE must be obtained for all other uses, in any current or future media, including reprinting/republishing this material for advertising or promotional purposes, creating new collective works, for resale or redistribution to servers or lists, or reuse of any copyrighted component of this work in other works.

Reuse

Items deposited in White Rose Research Online are protected by copyright, with all rights reserved unless indicated otherwise. They may be downloaded and/or printed for private study, or other acts as permitted by national copyright laws. The publisher or other rights holders may allow further reproduction and re-use of the full text version. This is indicated by the licence information on the White Rose Research Online record for the item.

Takedown

If you consider content in White Rose Research Online to be in breach of UK law, please notify us by emailing eprints@whiterose.ac.uk including the URL of the record and the reason for the withdrawal request.



eprints@whiterose.ac.uk
<https://eprints.whiterose.ac.uk/>

A Pneumatic Anchoring Mechanism for Improved Stability in Soft Magnetic Manipulators for Surgery

Zaneta Koszowska, Michael Brockdorff, Peter Lloyd, James H. Chandler, *Member IEEE*, and Pietro Valdastri, *Fellow IEEE*

Abstract— This paper presents a synergistic soft robotic actuation approach, whereby pneumatically induced anchoring is applied to a Soft Magnetic Manipulator (SMM) to enable improved post navigation stability and tip manipulation accuracy. A SMM is equipped with an integrated pneumatic expansion chamber (anchor) and tool channel to enhance stability during interventional procedures. The pneumatic anchor is tested for its position-locking effectiveness during SMM tip loading. Additionally, tip manipulation stability with and without the anchoring system activated is assessed by measurement of the SMM’s ability to trace a parametric circle using an integrated laser fiber. The anchoring mechanism showed a mean improvement in tip actuation accuracy of 73.26%. The system is further demonstrated in the case study of a brain phantom, with the prototype equipped with a laser fiber. The SMM was navigated through a brain fold through application of external magnetic fields exploiting the dual External Permanent Magnet (dEPM) platform. Upon arrival at target site, the anchor was deployed to stabilize the SMM’s tip while laser targeting was performed, demonstrating the potential of this approach for procedures requiring high precision.

Index terms – Soft Robots, Magnetic Robot, Anchoring Mechanism

I. INTRODUCTION

Minimally Invasive surgery (MIS) when accessing brain lesions provides major benefits over an open skull surgery. MIS approaches work well for brain tumors or aneurysms located near the brain surface or where access is possible via a straight path. However, in cases where tumors are located in areas of the brain where straight tool trajectory would lead to penetration of brain tissues crucial in function, this approach is not feasible. In such cases, surgeons either opt for a traditional open craniotomy approach or simply deem the tumor inaccessible [1].

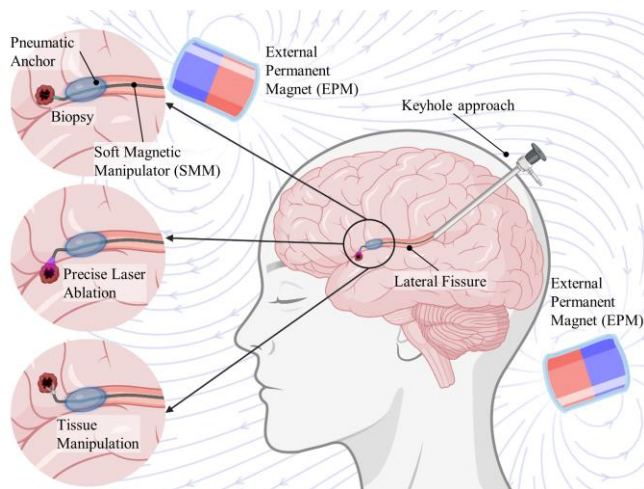


Figure 1. Proposed Soft Magnetic Manipulator (SMM) with pneumatic anchor, in a dEPM set up, enabling potential applications

in Minimally Invasive Surgery such as biopsy, precise laser ablation and tissue manipulation.

The field of soft robotics is facilitating expansion of keyhole surgery in the brain, for deeper brain access [2], [3]. Soft continuum robots, usually driven by means of pneumatics [4]–[6] or hydraulics [7], [8], and manufactured with elastomeric materials offer greater flexibility and less traumatic tissue interaction over current endoscopic tools [9]. This can open the possibility of navigating to the targeted area, between brain folds (known as sulci and fissures), as opposed to penetrating through the brain volume, allowing access to brain tumors located in difficult areas and significantly minimizing invasiveness of such procedures. This ensures that collateral damage to brain areas responsible for vital functions is minimized during surgery. While the concept of utilizing elastomeric devices is promising to overcome limitations in neurosurgery, there are numerous outstanding challenges. The available DoFs using popular actuation methods in soft structures are limited, especially at the required scale. Miniaturization of such devices to millimeter scale, is challenging due to the limits of scaling down the components of actuating systems such as air connections, tubing, wires etc. This becomes even more significant in devices requiring high maneuverability, where more components are implemented in the design [10].

Stimuli-responsive materials can induce shape deformation under external actuation trigger such as magnetic field, pH gradient, ultrasonication or temperature. The significant advantage of such materials is in miniaturization potential, since they often eliminate the need for onboard actuation components such as motors, wires, pressure connections or tubing. An example of a smart material that can be applied in medical devices is in Soft Magnetic Manipulators (SMMs), where the addition of magnetic particles to an elastomeric matrix, makes them responsive to external magnetic fields. This has been explored in medical applications by multiple research groups [11]–[13]. The miniaturization potential of SMMs combined with the material modulus close to that of soft tissue present clinical benefits including minimized interaction with the surrounding anatomy and deep access to human body [9], [14]. SMMs can be divided into two categories: tip magnetized and continuously magnetized. Magnetization along the length of the manipulator’s body can be either axial or off-axis, providing a signature magnetic profile, e.g. suited for a specific anatomy or patient as in [15], [16], making them a good fit for navigating in complex paths. Tip magnetized manipulators, however, are better suited for applications in less tortuous pathways, where tip maneuverability and/or simplicity of operation is prioritized. The advantage of this approach is that due to the simple magnetic profile the tip can be easily controlled in multiple Degrees Of Freedom (DoFs) with magnetic gradients, even

with a handheld magnet as in [17]. This multi-DoF tip actuation is challenging for continuously magnetized SMMs, due to the fundamental connection between internal magnetization and external applied field. Movement of the whole SMM's length when attempting tip only actuation is inevitable. Even if magnetic separation were possible, the movement of the tip would lead to uncontrollable movement of the more proximal region of the body due to their mechanical connection. Due to this phenomenon, applying stiffening approaches in SMMs would not only improve stability for high-payload tasks but also enable the highly desirable separation of the tip actuation from actuation of the SMM's body.

Structural compliance and softness are beneficial during navigation in delicate tissues, however, in cases where a procedure requires localized and accurate tip control could present itself as a disadvantage. Due to the compliant nature of elastomeric robotic devices, tasks such as biopsy can also pose challenges due to material buckling under load. Addressing this pivotal challenge in soft robotics has led to numerous efforts aimed at stiffening soft robots on demand. Temperature responsive materials [18], various material jamming and locking techniques [19]–[22] and even embedded chain mail [23] have all been demonstrated but invariably suffer from difficulties either related to unsafe transition temperatures or challenges in miniaturization [24]. For devices to gain needed stability to transmit forces essential to perform surgical tasks, researchers have also explored mechanical anchoring approaches such as pneumatic balloon [25], mechanical expandable structure [26] or magnetic anchoring [27], [28].

In this work, we present a novel design of a soft magnetic manipulator (SMM) aimed at improving movement stability and independent tip control during magnetic actuation. We modified previously presented SMM design [16] by adding a fully integrated pneumatic chamber, inspired by balloon catheters used to anchor within anatomical structures. This monolithic design facilitates smooth navigation and

deployment of the anchor on demand. Inflated anchor allows for independent control of the tip, stabilizing the rest of the device in the anatomy, when the tip is in motion (Fig. 1). Additionally, the tip can be actuated with precision, as the balloon functions as a stiffened section, comparable to approaches presented above. This prevents movements from the proximal SMM body from being transmitted beyond the balloon to the tip, which would otherwise cause disturbances in standard actuation scenarios without an anchoring mechanism.

Hence, by combining pneumatic anchoring with magnetic manipulation, our approach improves post-navigation stability and tip accuracy, offering a more controlled and stable magnetic actuation solution.

II. PNEUMATIC-MAGNETIC MULTI-MODAL SMM APPROACH

The presented prototype is 4 mm in diameter, with a thinner tip (2 mm) for improved deflection. The length of the tip is 15 mm, and the whole manipulator is 30 mm long. Design parameters of this prototype are guided by the clinical application of navigating through and anchoring in the lateral fissure of the brain, which varies between ~5.5 mm to 9 mm in a deformable surgical training simulator used in this work (UpSurgeOn, Italy). However, the length of maneuverable tip, as well as balloon diameter and wall thickness can be adjusted at the design stage depending on specific application, and the size of lumen/cavity in which the anchor will be deployed.

III. OPERATIONAL PRINCIPLES

A. Principles of Magnetic Actuation

A magnetic agent with magnetization $\boldsymbol{\mu} \in \mathbb{R}^3$ is subject to a magnetic force ($\boldsymbol{f} \in \mathbb{R}^3$) and torque ($\boldsymbol{\tau} \in \mathbb{R}^3$) under an applied field $\boldsymbol{B} \in \mathbb{R}^3$, respectively as:

$$\boldsymbol{f} = \nabla(\boldsymbol{\mu} \cdot \boldsymbol{B}) \quad (1)$$

$$\boldsymbol{\tau} = \boldsymbol{\mu} \times \boldsymbol{B} \quad (2)$$

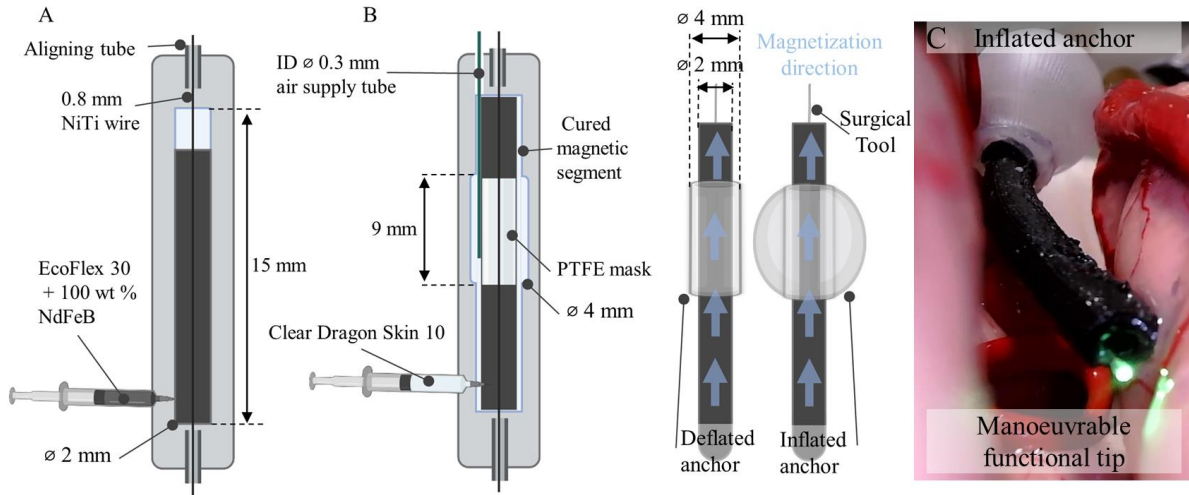


Figure 2. A. Molding process of the 2 mm magnetic core with a tool channel. B. Molding process of the pneumatic chamber, by injecting a layer of clear silicone over the cured magnetic core, in a secondary mold with cavity for chamber of 4 mm in diameter. C. Prototyped SMM with the deployed anchor and laser fiber in the tool channel.

where ∇ is the gradient operator. The magnetization vector(s) of an SMM is a crucial element when it comes to magnetic actuation of soft structures. According to Equation (2) when the magnetization μ of the magnetic body aligns with the applied external magnetic field direction, it is subject to no resultant torque (no actuation). If the direction of μ is not parallel with the external magnetic field vector B a resultant magnetic torque will be present on the body; expressed as the cross product of the magnetization direction and applied external magnetic field (2). Using this phenomenon, a SMM can be pre-programmed in a manner to achieve desired deformation, when exposed to specific external magnetic fields.

B. Pneumatic Chamber Design and Fabrication

Pneumatic actuators commonly feature chambers in a form of hollow silicone structures, utilizing their axial space for inflation. However, in the context of functionalizing the core of the SMMs a different approach is required. Here, to pass surgical tools, the inflating chamber must be either offset from center or placed concentrically around the device.

Fabricating the chamber separately from the SMM and assembling it with prefabricated magnetic segments poses multiple challenges in terms of the process and assembly.

Therefore, a standard fabrication technique for magnetic segment with tool channels as in e.g. [16] was adapted to cast the balloon around the SMM. This modification additionally enhances the versatility of the proposed system, enabling its integration with various types of SMMs.

The anchor consisting of a pneumatic chamber was designed to fit around a 2 mm magnetic segment. The anchor is fully integrated into SMM, meaning that the diameter of the core segment defines the diameter of the chamber core. The first step involved fabricating a magnetic segment of 2 mm diameter and 15 mm in length, by casting, with 3D printed molds (Grey V4 resin, Form III, Formlabs III, USA). Equal parts of elastomer (EcoFlex 30, Smooth-On, Inc., U.S.A.) A and B were mixed with 100 wt% of hard magnetic micro-particles (Nd-FeB with an average 5 μm diameter and intrinsic coercivity of $H_{ci} = 9.65$ kOe, MQFP-B+, Magnequench GmnH, Germany). The magnetic slurry was then mixed in a high vacuum-mixer (ARV- 310, ThinkyMixer, Japan) for 90 seconds at a speed of 1400 rpm and pressure of 20.0 kPa. The degassed mixture was injected into closed cylindrical molds with a 0.8 mm NiTi wire fixed concentrically along the length of the cavity to create a tool channel. The part was cured at 45°C for 30 minutes.

PTFE tape (75 μm thick by 9 mm wide) was wrapped around the mid part of the magnetic segment to act as a mask in a second stage of the molding process, as in [25]. The silicone-silicone bond can only be achieved in areas where no PTFE is applied, creating a chamber where the mask is present, as depicted in Figure 2.

The magnetic segment with applied mask was aligned in the secondary mold, ensuring that the vertical NiTi wire was placed in the alignment slots on both sides of the mold. The alignment is crucial to create a chamber with even wall thickness, allowing for uniform inflation and concentric balloon profile. This was ensured by printing molds with alignment slots using 25 μm layer thickness in 3D printer

settings. Additionally steel tubes with (ID) of 0.9 mm were pressure fit into the alignment cavities in the molds. The steel tubes accommodate the 0.8 mm NiTi, passing through the segment providing concentric alignment of the core in the mold (Figure 2). A silicone tube (0.3 mm ID and 0.5 mm OD) was aligned on top of the magnetic segment as an air inlet and secured with an extra layer of PTFE. This was passed through a hole designed in the mold beforehand. 0.2 mm NiTi wire was inserted into the air inlet tube to prevent silicone blocking the tube while injecting. The mold was closed and clamped, followed by injection with a clear (undoped) layer of DragonSkin 10 Slow (Smooth-On, Inc., U.S.A). Upon careful demolding, NiTi wires were removed from the air supply tube and from the core.

EcoFlex 30 was chosen as the material for the core and tip because of its low elastic modulus and consequent capability to achieve high deflection angles, even when mixed with 100% NdFeB [29]. The balloon was molded with DragonSkin 10 due to improved durability upon inflation, as compared to EcoFlex materials.

This fabrication process resulted in a 4 mm SMM with a 2 mm magnetic core, 0.8 mm tool channel and inflatable chamber with a wall thickness of 1 mm as shown in Figure 2. This process can be easily adapted to suit various surgical demands for the SMM, including total diameter, tool channel size, as well as different geometries of the balloon.

IV. RESULTS

A. Anchoring experiment

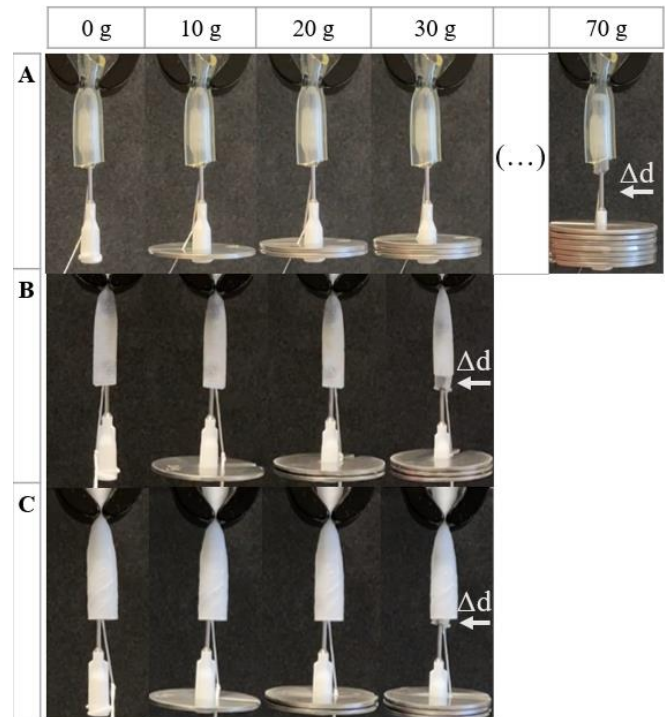


Figure 3. A mass was hung from the inflated SMM anchored in tubes of different diameters and lubrication. Results of anchoring evaluation tests where Δd is SMM's displacement; A. Dry 6 mm

silicone tube. B 6 mm (ID) Carotid Artery Phantom. C. 10 mm (ID) Saphenous Vein Phantom.

A representative prototype was evaluated for its anchoring strength by incrementally loading the inflated SMM. To simulate clinically relevant experimental conditions, the prototype was tested in phantoms with mechanical properties resembling those of human tissues, including a 6 mm (ID) Carotid Artery Phantom and 10 mm (ID) Saphenous Vein Phantom (Syndaver, USA), as well as a dry silicone tube with 6mm ID. The phantoms were kept in water with dish soap as per manufacturers guide. In each experiment, a phantom was secured vertically, and the anchor was deployed by supplying the chamber with 12 ml of air volume. The pneumatic connections were maintained the same throughout all experiments. Incremental loads (10 g) were added to the tip of the SMM until anchor was displaced, Δd (Figure 3).

Figure 3 shows that the tested prototype supported the most mass at the tip in a dry tube of 6 mm. The anchor failed at 70 g load. Lower friction in the phantoms in comparison to a dry tube caused the balloon to slip out of the lumens at 30 g load in both tested phantoms.

B. Tip manipulation independence

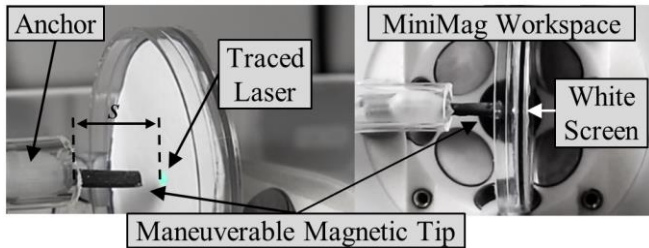


Figure 4. Experimental set-up for testing manipulation independence of the SMM's tip, including MiniMag Workspace, phantom tube, SMM with an inflated anchor and screen for laser tracing.

To assess the independence of magnetically manipulating the SMM's tip with the inflated anchor, a series of tests were performed under transient, homogeneous magnetic actuation. The prototyped manipulator was equipped with a multimode

laser fiber with a total diameter of 0.5 mm (0.39 NA TECS-Clad Multimode Optical Fiber, ThorLabs, USA).

The SMM was placed in lumens (as in Section IV A) aligned in omnidirectional magnetic field generation platform (MGF-100, MagnebotiX, Switzerland) [30] originally along the X axis of the platform. An orthogonal field (in the Y-Z plane) was rotated about the SMM's long axis ($|\mathbf{B}| = 20$ mT, 0.5 Hz), a field which should theoretically draw a circle with the laser on a flat target oriented in the YZ plane.

The anticipated diameter of the circle was calculated based on a balance between magnetic torque (left hand side of equation 3) and beam bending torque (right hand side of equation 3), adapted from [31]:

$$\mathbf{m} \times \mathbf{B} = \frac{EI}{L} \theta \quad (3)$$

Where \mathbf{m} is the magnetic moment of the manipulator (Am^2), \mathbf{B} the applied field (T), E the elastic modulus of the beam (Nm^{-2}), L the unconstrained length of the beam (15 mm) and I the second moment of area of the bending beam (m^4), defined as:

$$I = \frac{\pi d^4}{64} \quad (4)$$

The stiffness of the entire beam is the sum of the stiffnesses of the component parts, namely, the elastomer ($d_{\text{outer}} = 2$ mm, $d_{\text{inner}} = 0.8$ mm, $E = 360$ kPa [29]), the laser ($d = 0.2$ mm, $E = 50$ GPa [32]) and the Teflon sheath surrounding the laser ($d = 0.5$ mm, $E = 500$ MPa [33]). Theta is the bending angle of the beam giving, assuming linearity, the resultant radius of the laser sketched circle of:

$$r_{\text{circle}} = s \cdot \sin\left(\mathbf{m} \times \mathbf{B} \cdot \left(\frac{L}{EI}\right)\right) \quad (5)$$

With s the distance from the base of the SMM's tip to the screen (Fig. 4). The data on the laser position was continuously captured with a camera (Basler, Germany) and repeated with the deflated and inflated anchor (12 ml air volume), in 3 phantom lumens. Figure 5 presents the analysis of collected data, comparing laser points captured with camera to an expected circle based on Equation 5.

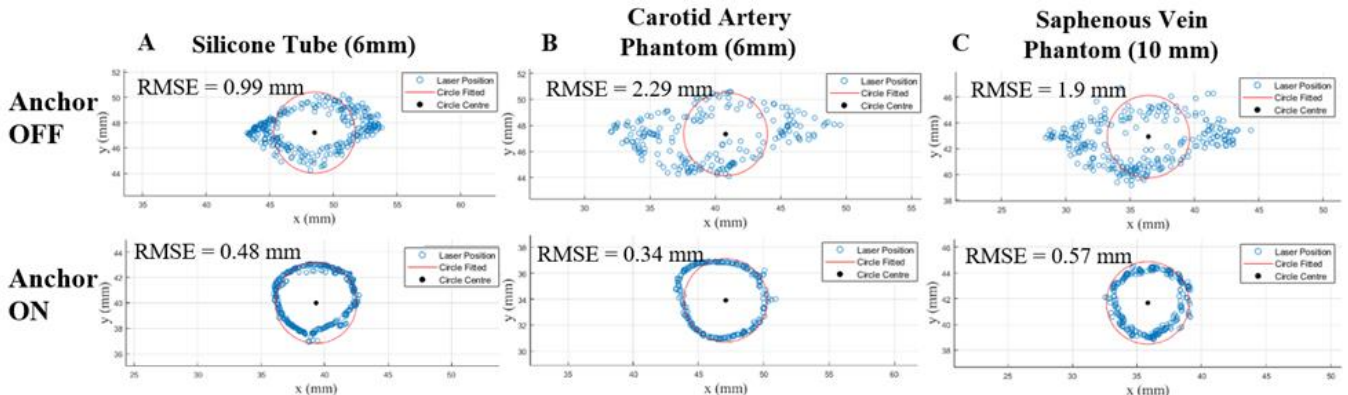


Figure 5. Results of a circle drawing task by anchored and unanchored SMMs in the MiniMag workspace under the same rotating magnetic field conditions $B_z = 20$ mT, 0.5 Hz. A. Silicone Tube 6 mm ID – dry. B. Lubricated Carotid Artery Phantom 6mm ID. C. Lubricated Saphenous Vein Phantom 10 mm ID.

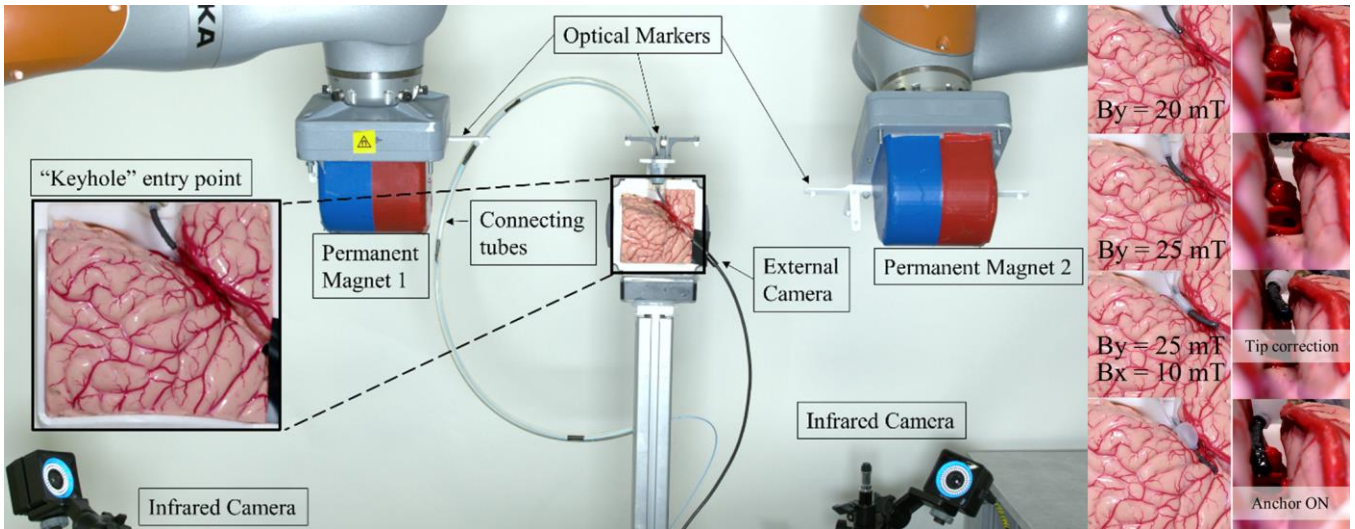


Figure 6. A. Experimental set-up including dual External Permanent Magnet (dEPM) platform, optical tracking system for calibration, brain phantom and SMM with its connections. B. Results of SMM testing in the brain phantom. From the top: navigation into the brain fold with manual insertion and magnetic field application, tip correction and inflation. More details in Supplementary Video 1.

It can be observed that the unanchored SMM was unable to draw a circle in all three tested cases. Collected data with unanchored SMM for “Silicone tube 6 mm” condition shows the drawn shape being the closest to the target circle from all tested cases. The average Root Mean Square Error (RMSE) for the “Anchor OFF” condition was 1.72 mm while for the “Anchor ON” it was 0.46 mm, showing reduction of the average RMSE of 73.26%.

V. CASE STUDY: DEMONSTRATION IN A BRAIN PHANTOM

To demonstrate clinical applicability of the proposed prototype, the system was tested in a brain phantom. The clinical assumption was made such that in a real case scenario, the SMM would enter through a keyhole in the skull, drilled aligned to a plane of the targeted brain fold, as the concept drawing in Figure 1 [1]. Following clinical requirements to access brain fold workspace, the manipulator in most cases follows a similar trajectory, navigating along the brain fold then bending inwards. In this paper we use a simulator of the brain with exposed lateral fissure. Hence, in this case we opted for a standard magnetic profile, magnetizing the SMM along its length (Fig. 2). Axial magnetic profile in this case is sufficient, providing needed deflection to bend along the lateral fissure and maneuver the tip upon anchor inflation. The magnetic profile, however, could readily be generalized for more complex navigations, where off-axis magnetization would be required.

A neurosurgical brain simulator (upsurgeon.com; model: AneurysmBox) was fixed in the dual External Permanent Magnet (dEPM) set up (Figure 6). Frames with optical markers were mounted at the top of the simulator, and on the permanent magnets, to facilitate calibration of the dEPM platform [34]. An external camera was mounted pointing into the fissure for visual feedback during the experiment. The SMM with anchor and laser fiber passing through the tool channel, was attached to a silicone tube with Silpoxy adhesive (Smooth-On, Inc., U.S.A.). The SMM was manually inserted

into the workspace while applying magnetic field conditions: $B_y = [20 \text{ mT}; 25 \text{ mT}]$, (Figure 5B) (Table 1). At the last insertion step, additional field $B_x = [10 \text{ mT}]$ was applied to straighten the tip into required position (this can be seen in the Supplementary Video 1).

After insertion, the inflating mechanism was deployed by supplying the chamber with 12 ml of air, to stabilize the SMM to achieve actuation independence of the tip. The tip was then actuated by applying magnetic field conditions as in Table 1. This demonstration showed tip actuation as desired, without movement of the rest of SMM body. This can be seen in the Supplementary Video 1.

Table 1. Magnetic field conditions applied in the phantom

	B_x	B_y	B_z
Insertion	0	20 mT	0
	0	25 mT	0
Tip correction	10 mT	25 mT	0
Tip actuation	- 5 mT	0	0
	- 5 mT	15 mT	0
	- 5 mT	25 mT	0
	- 5 mT	10 mT	0
	- 5 mT	15 mT	0
		15 mT	0
	-10 mT	15 mT	0
	5 mT	15 mT	0
-5 mT	15 mT	0	

DISCUSSION AND FUTURE WORK

In this work, we presented a novel anchoring mechanism for SMMs, aiming at stabilizing a manipulator’s body during surgical procedures, to allow independent and accurate actuation of the tip.

The experimental testing to evaluate anchoring strength of the presented approach, showed that the design can support up to

70 g load at the tip for a dry tube and up to 30 g in lubricated phantom lumens. This shows a potential to use the anchor in medical settings where high payload at the tip is applied. In the future this capability should be further investigated and exploited by performing tasks requiring a payload at the tip, such as biopsy and penetration tasks (e.g. injections) in soft tissues. Additionally, the phantoms should be tested for their tribological properties to accurately evaluate anchoring properties depending on surface friction. It could be also beneficial to measure tissue deformation while the anchor is on. The results provided for independent tip evaluation show improved accuracy of targeted motion in all tested cases with anchored SMM. Inaccuracies in control without anchor vary depending on the size of the lumen, as expected. However, in all presented cases, the anchor improved the accuracy of tip motion, 73.26 % on average. The RMSE is larger for unanchored SMM in phantom tubes. This is likely caused by the lubrication of lumens, creating more challenging conditions for anchoring, as opposed to the dry silicone tube. The uneven shape of resultant tracked motion for the “Anchor OFF” condition observed in Figure 4 is caused by rotation of the body length of the SMM under the rotating field. Due to the lack of anchor, the whole body of the SMM twists in the tube, allowing for magnetic gradient to pull it towards bottom left side of the workspace, while it is turning clockwise and thus creates a skewed and noisy shape. It should be noted that all results presented in this work correspond to one design of the SMM, featuring specific design parameters such as length, diameter, base material, and concentration of magnetic particles. Variation of these parameters will likely affect the maneuverability as well as stability when the anchor is on. Clinical applicability was further demonstrated in a case study of a brain simulator, showing successful navigation with magnetic actuation, inflation in the lateral fissure and independent tip actuation. For feedback while navigating in clinical scenarios, future research should involve using Fiber-Bragg sensors or similar running along the main axis of the manipulator. This can provide a non-visual shape-feedback when navigating deep in the brain tissue, and therefore beyond visual range. Additionally, since NdFeB particles are cytotoxic, further investigation should involve either biocompatible coatings of the whole SMM or magnetic components prior to the fabrication process, or an alternative biocompatible hard magnetic material [35]. This system shows potential to be applied in a broad range of medical procedures, where stability is important, such as laser ablation, biopsies and tissue retrieval. The placement of the anchor can be adjusted to suit the length requirements of segments that need to be separated. For applications where longer SMMs would be more beneficial, multiple balloons can be implemented for improved stability in a longer body. It would be of interest to implement multiple balloons and depending on required tip length in specific application, selectively activate, thus controlling the length of the unconstrained tip. The chamber design can be adjusted to

anchor in various lumen diameters.

ACKNOWLEDGMENT

Research reported in this article was supported by the Engineering and Physical Sciences Research Council (EPSRC) under grants number EP/R045291/1 and EP/V009818/1, and by the European Research Council (ERC) under the European Union’s Horizon 2020 research and innovation programme (grant agreement No 818045). Any opinions, findings and conclusions, or recommendations expressed in this article are those of the authors and do not necessarily reflect the views of the EPSRC or the ERC.

REFERENCES

- [1] W. S. Cho, J. E. Kim, H. S. Kang, Y. J. Son, J. S. Bang, and C. W. Oh, “Keyhole approach and neuroendoscopy for cerebral aneurysms,” *J. Korean Neurosurg. Soc.*, vol. 60, no. 3, pp. 275–281, 2017, doi: 10.3340/jkns.2017.0101.002.
- [2] M. Runciman, A. Darzi, and G. P. Mylonas, “Soft Robotics in Minimally Invasive Surgery,” *Soft Robot.*, vol. 6, no. 4, pp. 423–443, 2019, doi: 10.1089/soro.2018.0136.
- [3] T. Amadeo *et al.*, “Soft Robotic Deployable Origami Actuators for Neurosurgical Brain Retraction,” *Front. Robot. AI*, vol. 8, no. January, pp. 1–12, 2022, doi: 10.3389/frobt.2021.731010.
- [4] J. H. Chandler, M. Chauhan, N. Garbin, K. L. Obstein, and P. Valdastrì, “Parallel Helix Actuators for Soft Robotic Applications,” *Front. Robot. AI*, vol. 7, no. September, pp. 1–17, 2020, doi: 10.3389/frobt.2020.00119.
- [5] M. McCandless, A. Perry, N. DiFilippo, A. Carroll, E. Billatos, and S. Russo, “A Soft Robot for Peripheral Lung Cancer Diagnosis and Therapy,” *Soft Robot.*, vol. 00, no. 00, pp. 1–13, 2021, doi: 10.1089/soro.2020.0127.
- [6] I. De Falco, M. Cianchetti, and A. Menciassi, “A soft multi-module manipulator with variable stiffness for minimally invasive surgery,” *Bioinspiration and Biomimetics*, vol. 12, no. 5, 2017, doi: 10.1088/1748-3190/aa7ccd.
- [7] J. Fras, Y. Noh, M. Macias, H. Wurdemann, and K. Althoefer, “Bio-Inspired Octopus Robot Based on Novel Soft Fluidic Actuator,” *Proc. - IEEE Int. Conf. Robot. Autom.*, pp. 1583–1588, 2018, doi: 10.1109/ICRA.2018.8460629.
- [8] F. Campisano *et al.*, “Teleoperation and Contact Detection of a Waterjet-Actuated Soft Continuum Manipulator for Low-Cost Gastroscopy,” *IEEE Robot. Autom. Lett.*, vol. 5, no. 4, pp. 6427–6434, 2020, doi: 10.1109/LRA.2020.3013900.
- [9] T. Veiga *et al.*, “Challenges of continuum robots in clinical context : a review,” pp. 1–39.
- [10] P. E. Dupont *et al.*, “A decade retrospective of medical robotics research from 2010 to 2020,” *Sci. Robot.*, vol. 6, no. 60, 2021, doi: 10.1126/scirobotics.abi8017.
- [11] G. Z. Lum *et al.*, “Shape-programmable magnetic soft matter,” *Proc. Natl. Acad. Sci. U. S. A.*, vol. 113, no. 41, pp. E6007–E6015, Oct. 2016, doi: 10.1073/pnas.1608193113.
- [12] Z. Li, O. Youssefi, and E. Diller, “Magnetically-guided in-situ microrobot fabrication,” *IEEE Int. Conf. Intell. Robot. Syst.*, vol. 2016-Novem, pp. 5131–5136, 2016, doi: 10.1109/IROS.2016.7759753.
- [13] J. Hwang *et al.*, “An Electromagnetically Controllable Microrobotic Interventional System for Targeted, Real-Time Cardiovascular Intervention,” *Adv. Healthc. Mater.*, vol. 11, no. 11, 2022, doi: 10.1002/adhm.202102529.
- [14] Z. Li, J. Li, Z. Wu, Y. Chen, M. Yeerbulati, and Q. Xu, “Design and Hierarchical Control of a Homocentric Variable-Stiffness Magnetic Catheter for Multiarm Robotic Ultrasound-Assisted Coronary Intervention,” *IEEE Trans. Robot.*, vol. 40, pp. 2306–2326, 2024, doi: 10.1109/TRO.2024.3378442.
- [15] P. Lloyd *et al.*, “A learnt approach for the design optimisation of magnetically actuated shape forming soft tentacle robots,” 2019.
- [16] G. Pittiglio *et al.*, “Personalized magnetic tentacles for targeted

- photothermal cancer therapy in peripheral lungs,” pp. 1–13, 2023, doi: 10.1038/s44172-023-00098-9.
- [17] Y. Kim, G. A. Parada, S. Liu, and X. Zhao, “Ferromagnetic soft continuum robots,” 2019. [Online]. Available: <http://robotics.sciencemag.org/>.
- [18] Y. Piskarev *et al.*, “Fast-Response Variable-Stiffness Magnetic Catheters for Minimally Invasive Surgery,” vol. 2305537, pp. 1–14, 2024, doi: 10.1002/advs.202305537.
- [19] M. Brancadoro, M. Manti, F. Grani, S. Tognarelli, A. Menciasci, and M. Cianchetti, “Toward a variable stiffness surgical manipulator based on fiber jamming transition,” *Front. Robot. AI*, vol. 6, no. MAR, pp. 1–12, 2019, doi: 10.3389/frobt.2019.00012.
- [20] D. S. Shah, E. J. Yang, M. C. Yuen, E. C. Huang, and R. Kramer-Bottiglio, “Jamming Skins that Control System Rigidity from the Surface,” *Adv. Funct. Mater.*, vol. 31, no. 1, 2021, doi: 10.1002/adfm.202006915.
- [21] B. Yang *et al.*, “Reprogrammable soft actuation and shape-shifting via tensile jamming,” *Sci. Adv.*, vol. 7, no. 40, pp. 1–11, 2021, doi: 10.1126/sciadv.abh2073.
- [22] J. Liu, L. Yin, J. H. Chandler, X. Chen, P. Valdastrì, and S. Zuo, “A dual-bending endoscope with shape-lockable hydraulic actuation and water-jet propulsion for gastrointestinal tract screening,” *Int. J. Med. Robot. Comput. Assist. Surg.*, vol. 17, no. 1, pp. 1–13, 2021, doi: 10.1002/rcs.2197.
- [23] Y. Wang, L. Li, D. Hofmann, J. E. Andrade, and C. Daraio, “Structured fabrics with tunable mechanical properties,” *Nature*, vol. 596, no. 7871, pp. 238–243, 2021, doi: 10.1038/s41586-021-03698-7.
- [24] M. Manti, V. Cacucciolo, and M. Cianchetti, “Stiffening in soft robotics: A review of the state of the art,” *IEEE Robot. Autom. Mag.*, vol. 23, no. 3, pp. 93–106, 2016, doi: 10.1109/MRA.2016.2582718.
- [25] D. Van Lewen, T. Janke, H. Lee, R. Austin, E. Billatos, and S. Russo, “A Millimeter-Scale Soft Robot for Tissue Biopsy Procedures,” *Adv. Intell. Syst.*, vol. 5, no. 5, 2023, doi: 10.1002/aisy.202200326.
- [26] J. Rogatinky *et al.*, “A multifunctional soft robot for cardiac interventions,” *Sci. Adv.*, 2023, doi: 10.1126/sciadv.adi5559.
- [27] W. Li, T. Cheng, M. Ye, C. S. H. Ng, P. W. Y. Chiu, and Z. Li, “Kinematic Modeling and Visual Servo Control of a Soft-Bodied Magnetic Anchored and Guided Endoscope,” *IEEE/ASME Trans. Mechatronics*, vol. 25, no. 3, pp. 1531–1542, 2020, doi: 10.1109/TMECH.2020.2978538.
- [28] T. Cheng, X. Zhang, C. S. H. Ng, P. W. Y. Chiu, and Z. Li, “Design and Evaluation of a Soft-Bodied Magnetic Anchored and Guided Endoscope,” *J. Med. Robot. Res.*, vol. 03, no. 03n04, p. 1841007, 2018, doi: 10.1142/s2424905x18410076.
- [29] T. Da Veiga *et al.*, “Material Characterization for Magnetic Soft Robots.”
- [30] O. Khatib, V. Kumar, and G. Sukhatme, “MiniMag: A Hemispherical Electromagnetic System for 5-DOF Wireless Micromanipulation,” *Springer Tracts Adv. Robot.*, vol. 79, pp. 317–318, 2014, doi: 10.1007/978-3-642-28572-1.
- [31] P. Lloyd, G. Pittiglio, J. H. Chandler, and P. Valdastrì, “Optimal Design of Soft Continuum Magnetic Robots under Follow-the-leader Shape Forming Actuation,” pp. 111–117, 2021, doi: 10.1109/ismr48331.2020.9312943.
- [32] Schott Advanced Optics, “Mechanical and thermal properties of optical glass,” *Tie-31*, no. October, pp. 1–8, 2018.
- [33] Ideal-tek, “Engineering plastic type PTFE, Technical data sheet,” pp. 1–2.
- [34] G. Pittiglio, M. Brockdorff, T. da Veiga, J. Davy, J. H. Chandler, and P. Valdastrì, “Collaborative Magnetic Manipulation via Two Robotically Actuated Permanent Magnets,” *IEEE Trans. Robot.*, pp. 1–12, 2022, doi: 10.1109/TRO.2022.3209038.
- [35] A. Pena-Francesch *et al.*, “Macromolecular radical networks for organic soft magnets,” *Matter*, 2024, doi: 10.1016/j.matt.2023.12.015.